Chapter 5

Shape Memory Alloy Patches for Structural Repair

5.1 Introduction

There has always been interest in finding new methods to repair and mitigate damage in cracked structures and recently this interest was directed towards the use of SMA's. Research has been conducted on embedding SMA wires into an epoxy matrix and then looking at the ability of SMAs to close cracks within that matrix. Shimamoto *et al.* (1997), used embedded SMAs in epoxy resin to improve the fracture toughness of the composites as well as to determine whether active damage control of cracks in the SMA-epoxy system, was possible. These authors tensile pre-strained the SMA wires to 0, 1, 3 and 5% before embedment. The epoxy was then heated to a temperature above A_f resulting in the wires attempting to revert to their original length. This produced compressive stresses within the matrix. Side notches of several different lengths were cut into the SMA-epoxy specimen. Photoelastic fringes were then used to determine the reduction in the stress intensity factor around the notch tip. The results showed that the SMA wires can decrease the stress intensity factor at the notch tip by as much as 45%.

Fatigue crack propagation under tensile loading in a SMA-Al matrix system was

investigated by Furuya (1996). The specimens, with the embedded wires, were strained in order to induce a pre-strain in the wires. Furuya observed that the stiffness of the TiNi/Al composite was slightly increased compared with that of a pure Al specimen, due to the high stiffness of the TiNi wire. It was also found that the Al matrix failed before the TiNi fibres. Furuya showed that the crack propagation velocity decreased when the wires were heated to above their A_s temperature, attributed to the SMA shrinkage. The stiffness of the composite increased by 3% when the wires were heated above A_s for a V_f of 3% of TiNi fibres. At the crack tip, the TiNi fibres also undergo a SIM transformation due to the large stress concentrations around the tip, leading to a better resistance to fatigue failure.

However there has been little research conducted into the use of SMAs to repair cracks in existing structures. An investigation into the use of SMAs to close cracks in existing structures, by Yanliang *et al.* (1998), showed that by applying a thin NiTi film onto a cracked component and activating it, the strain at the crack tip was reduced by 18% and the stress intensity factor, K_I, was reduced by around 23%-29% depending on the stresses applied. Wang *et al.* (1999) calculated theoretical closure stresses for a SMA-composite and determined the optimum volume fraction of wires is required in order to produce the maximum closure stresses.

This chapter explores the possibility of using SMA-composites for the repair of existing cracked metallic structures. The thermomechanical results obtained from Chapter 3 for the recovery stresses of SMA composites are used and compared with the analytical solution determined by Wang *et al.* (1999) to obtain the magnitude of the recovery forces obtainable. A finite element model (FEM) of a SMA-composite, attached to a metallic substrate was investigated in order to determine the magnitude of stresses being transferred into the underlying structure to assess the feasibility of using such a patch. The FEM was developed on two frameworks: 1. Analytical modelling from Section 5.2 and 2. experimental results obtained from Chapter 3.

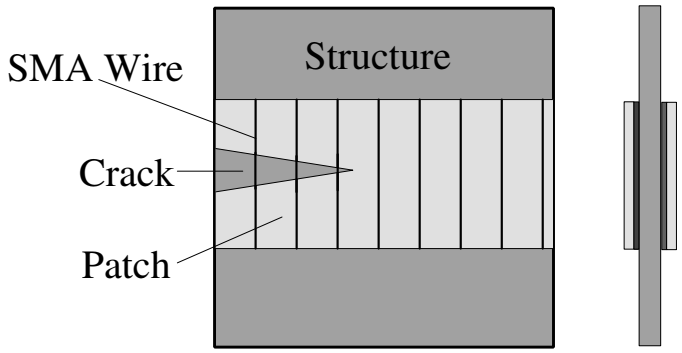

Figure 5.1: Schematic diagram of a cracked metallic structure with a SMA-composite patch applied to the surfaces.

5.2 Analytical Modelling of a SMA-Composite Patch

Figure 5.1 is a schematic diagram of a cracked metallic structure with a SMA patch applied to both sides of the cracked plate. A patch is applied to two sides in order to avoid complicated out of plane secondary bending.

Figure 5.2 shows the stresses which are acting on the patch and plate during the activation of the SMA wires. From these stresses the equilibrium equations 5.1 can be obtained.

$$\begin{aligned} \frac{d\sigma_p}{dx} + \frac{\tau_a}{h_p} &= 0 \\ \frac{d\sigma_s}{dx} - \frac{\tau_a}{h_s} &= 0 \end{aligned} \tag{5.1}$$

h_s and h_p are the thicknesses of the structure and patch, respectively, and τ_a is the shear stress in the adhesive layer.

The constitutive equations for each element, shown in Figure 5.2, are given in equation 5.2.

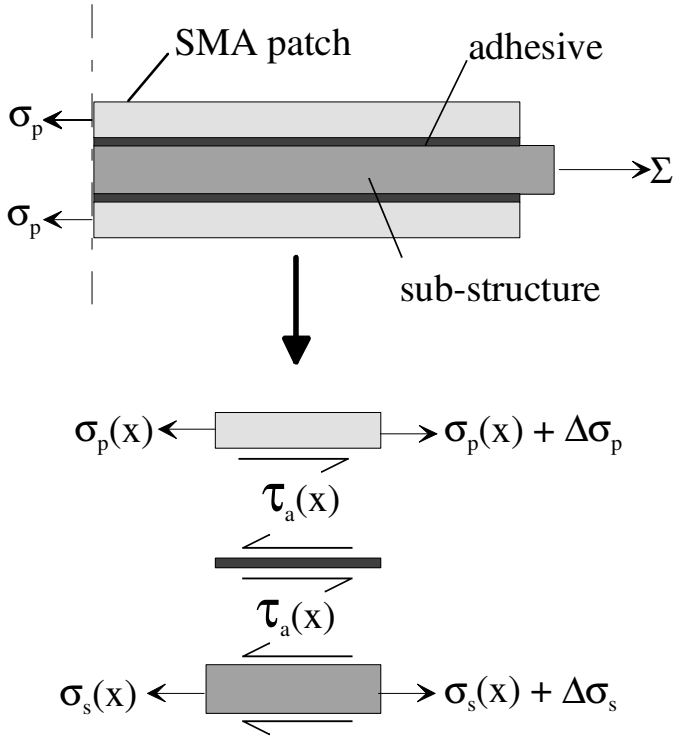

Figure 5.2: Schematic diagram of the stresses obtained from each of the elements in the cracked patched structure

$$\begin{aligned}
\text{SMA-Composite Patches:} \quad \sigma_p &= E_p\left(\frac{du_p}{dx} + \epsilon_p(\epsilon_{sma})\right) \\
\text{Adhesive Layers:} \quad \tau_a &= \frac{G_a}{h_a}(u_s - u_p) \\
\text{Cracked Structure:} \quad \sigma_s &= E_s\frac{du_s}{dx} \\
\text{SMA:} \quad \sigma_{sma} &= E_{sma}(\epsilon_p - \epsilon_{sma}) \\
\text{Kevlar Fibre/Epoxy Matrix:} \quad \sigma_m &= E_m(\epsilon_p - \epsilon_m)
\end{aligned} \tag{5.2}$$

where E_p is the Young's modulus of the patch, and can be calculated by equation 5.3. G_a is the adhesive shear modulus and E_s is the Young's modulus of the structure. σ_p is the average normal stress of the composite patches and σ_s is the average normal stress in the cracked structure. u_s and u_p are the in-plane displacements along the x-axis direction of the structure and the patches, respectively. $\epsilon_p(\epsilon_{sma})$ is the equivalent pre-strain in the patch with respect to the pre-strain in the SMA wires which is given

by equation 5.7 and ϵ_m is the strain in the matrix.

$$\begin{aligned} E_p &= \frac{A_{sma}}{A_T} n_w E_{sma} + \frac{A_m}{A_T} E_m \\ &= \frac{A_{sma}}{A_T} n_w E_{sma} + \frac{A_T - A_{sma}}{A_T} n_w E_m \\ &= \rho_{sma} E_{sma} + (1 - \rho_{sma}) E_m \end{aligned} \tag{5.3}$$

where

$$\rho_{sma} = \frac{A_{sma}}{A_T} \times n_w \tag{5.4}$$

.

and n_w is the number of embedded wires, A_{sma} and A_T are the cross sectional area of the SMA wires and the patch respectively.

The strain of the SMA wires is made up of the strain due to elastic loading, recoverable strain and strain due to thermal expansion effects as shown in equation 5.5. Similarly the matrix strain is given by equation 5.6. The pre-strain, ϵ_{ps}, induced in the SMA wires is the sum of the elastic (and, if any, plastic) and recoverable strains.

$$\begin{aligned} \epsilon_{sma} &= \epsilon_{se} + \epsilon_{sr} + \epsilon_{sa} \\ &= \epsilon_{ps} + \alpha_{sma}(T - T_0) \end{aligned} \tag{5.5}$$

$$\begin{aligned} \epsilon_m &= \epsilon_{me} + \epsilon_{ma} \\ &= \epsilon_{me} + \alpha_m(T - T_0) \end{aligned} \tag{5.6}$$

where the thermal coefficients of expansion of the SMA element and the Kevlar epoxy matrix are given by $\alpha_{sma} = 11 \times 10^{-6}$ and $\alpha_m = -3.6 \times 10^{-6}$ (Balta *et al*, 2001 and Schrooten *et al*, 2000), respectively. ϵ_{se}, ϵ_{sr} and ϵ_{sa} are the elastic strain, recoverable shape memory strain and thermal expansion strain of the shape memory alloys, respectively, and ϵ_{me} and ϵ_{ma} are the elastic and thermal expansion strains of the matrix material, respectively.

Thus, the following equation for the equivalent pre-strain is obtained.

$$\epsilon_p\left(\epsilon_{sma}\right) = \frac{\rho_{sma}(\epsilon_{ps} + \epsilon_{sa}) + (1 - \rho_{sma})\eta_m \epsilon_{ma}}{\rho_{sma} + (1 - \rho_{sma})\eta_m} \tag{5.7}$$

where

$$\eta_m = \frac{E_m}{E_{sma}}$$

By solving equations 5.1 and 5.2 the following relation can be obtained for the in-plane normal stress at the crack surfaces for a closed crack (Wang *et al.*, 1999):

$$\sigma_s(0) = \frac{1}{\kappa_s + \kappa_p}\left(\kappa_p + \frac{\kappa_s}{cosh\Lambda l_p}\right)\Sigma - \frac{\kappa_s}{\kappa_s + \kappa_p}\left(1 - \frac{1}{cosh\Lambda l_p}\right) E_s\, \epsilon_p\left(\epsilon_{sma}\right) \tag{5.8}$$

where l_p is the length of the SMA-composite patches, Σ is the external stress applied to the sub structure (as shown in Figure 5.2) and

$$\begin{aligned} \kappa_s &= \frac{1}{E_s h_s} \\ \kappa_p &= \frac{1}{E_p h_p} \\ \Lambda^2 &= \frac{(\kappa_s + \kappa_p) G_a}{h_a} \end{aligned} \tag{5.9}$$

For an open crack the result for the in-plane displacement normal to the crack surfaces is given by equation 5.10.

$$\begin{aligned} u_s(0) = \kappa_a h_s \Lambda cosh(\Lambda l_p) \Bigg[& \frac{1}{\kappa_s + \kappa_p}\left(\kappa_p + \frac{\kappa_s}{cosh\Lambda l_p}\right)\Sigma \\ & - \frac{\kappa_s}{\kappa_s + \kappa_p}\left(1 - \frac{1}{cosh\Lambda l_p}\right) E_s\, \epsilon_p\left(\epsilon_{sma}\right) \Bigg] \end{aligned} \tag{5.10}$$

where

$$\kappa_a = \frac{h_a}{G_a}$$

The first term in equations 5.8 and 5.10 is related to crack repair using patches (Rose (1982 and 1988)). The second term is due to the shape memory effect of the SMA-composite patch. The closure stress is thus given by:

Table 5.1: Material properties used for analytical calculations.

	SMA‡	Kevlar/Epoxy Matrix†	Aluminium	SMA-Patch
E(GPa)	62.7	33.5	70	30§
α (/°C)	11×10^{-6}	-3.6×10^{-6}	-	-

‡As a first approximation the SMA is assumed to be in it's austenitic state (at 140°C).
†53.5% Kevlar 29 fibre content and epoxy resin system, LTM217, 2 plys.
§From experiment, Table 3.8.

$$\sigma_c = \frac{\kappa_s}{\kappa_s + \kappa_p}\left(1 - \frac{1}{cosh\Lambda l_p}\right) E_s\,\epsilon_p\,(\epsilon_{sma}) \tag{5.11}$$

where

$$\Lambda l_p = \sqrt{\frac{l_p}{h_a}\left(\frac{G_a l_p}{E_s h_s} + \frac{G_a l_p}{E_p h_p}\right)} \gg 1 \tag{5.12}$$

Hence the closure stress can be simplified to

$$\sigma_c = \frac{\kappa_s}{\kappa_s + \kappa_p} E_s \epsilon_p\,(\epsilon_{sma}) \tag{5.13}$$

The closure stress is the stress which is transferred into the structure by the recovery stress of the embedded SMA.

5.3 Results

The material properties used are shown in Table 5.1. A SMA-wire with a diameter of 0.15 mm was used and the thickness of the cracked structure, h_s, ranged between 5-200 mm, and the thickness of the patch, h_p, from 0.2-0.8 mm (based on experiment). The width of the patch, w_p, was 10 mm, in order to be able to compare the results from the experiments shown in Chapter 3. For this investigation it was assumed that the patches were applied to a cracked aluminium structure.

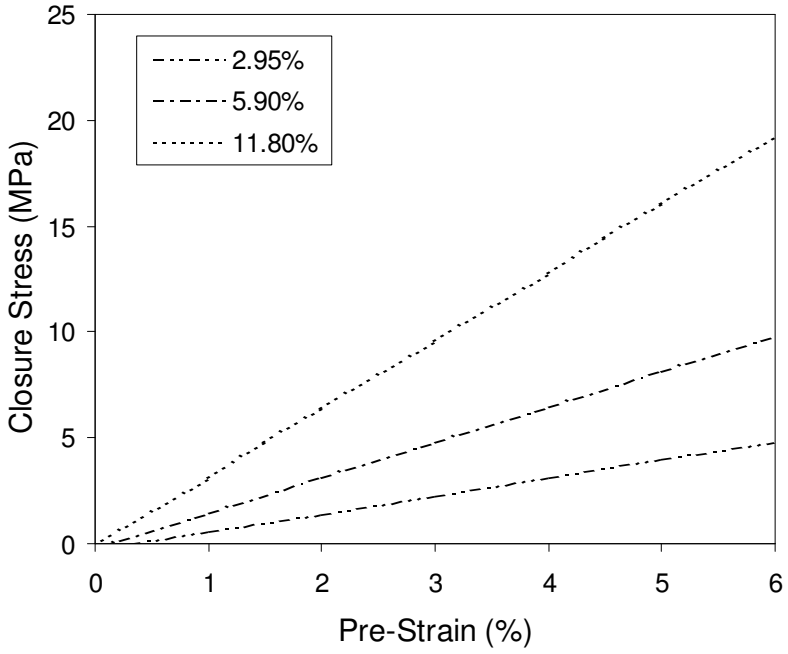

Figure 5.3: Closure stress versus pre-strain for varying V_f of SMA wires. The thickness of the patch, h_p, was 0.3 mm.

5.3.1 Closure Stress

Figure 5.3 shows the effect on σ_c with changing V_f of wires and pre-strains. As expected, σ_c increases with increasing pre-strain and V_f. It can also be noted that for low V_f the rate of increase of the closure stress with pre-strain decreases which is in agreement with the experimental results which showed that for low V_f there was a very small increase in the recovery stresses as pre-strain was increased.

Figure 5.4 shows the effect of varying the thickness of the patch and the cracked structure on σ_c. When the thickness of the structure is increased, σ_c decreases. If the cracked structure is too thick then the SMA recovery stresses will have little effect on closing a crack. For a constant V_f there is little difference in the closure stress for different patch thicknesses which is to be expected since the same V_f of wires will generate similar recovery stress when activated, regardless of the change in thickness of the patch. Figure 5.5 shows the variation in the closure stress for varying V_f with a

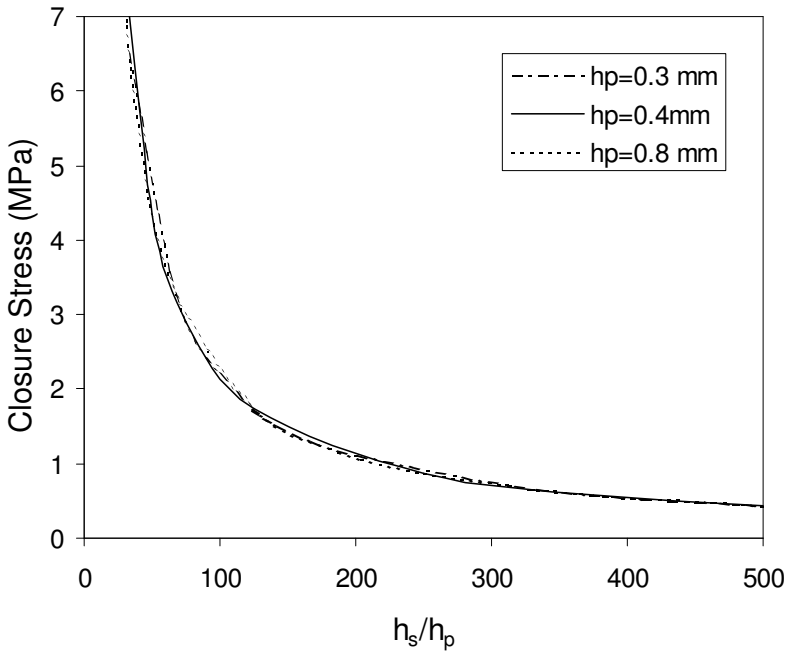

Figure 5.4: Closure stress versus thickness ratio for varying patch (h_p) and cracked structure (h_s) thickness, for wires pre-strained to 3% for a V_f of 11.8%.

patch thickness of 0.3 mm. From this it can be seen that for a V_f of 11.8% there is a larger closure stress generated compared to the lower pre-strain values.

An estimate of the maximum closure stress expected due to the recovery stresses in a SMA element can be obtained by equating the recovery force, F_r, with the transferred force, F_t, given by equations 5.14 and 5.15.

$$F_r = \sigma_r A_T \tag{5.14}$$

$$F_t = \sigma_c h_s w_s \tag{5.15}$$

where σ_r is the recovery stress, w_s is the width of the cracked structure and A_T is the cross sectional area of the SMA-patch. Thus the closure stress is given by equation 5.16.

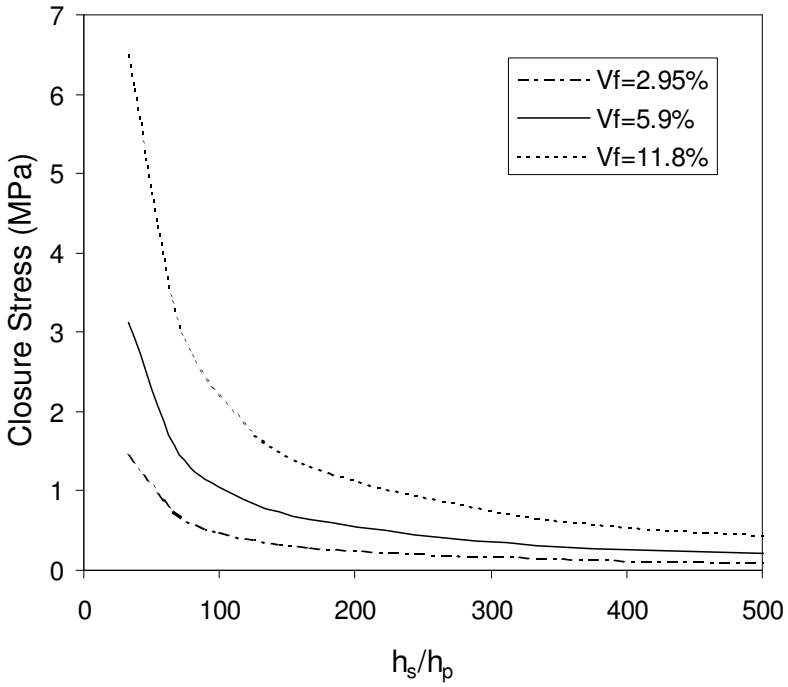

Figure 5.5: Closure stress versus thickness ratio for varying volume fraction of SMA wires, pre-strained to 3% and embedded in a patch of thickness 0.3 mm.

$$\sigma_c(max) = \frac{\sigma_r A_T}{h_s w_s} \tag{5.16}$$

This is the upper limit of the closure stress since it assumes that 100% of the force due to the recovery of the SMA elements is transferred into the structure.

Table 5.2 shows the results obtained for the maximum closure stress, $\sigma_c(max)$, for different pre-strains, based on the experimental results for σ_r found in Chapter 3. A comparison is also shown of the closure stresses, $\sigma_c(calc)$, obtained using the analytical solution. In order to compare the 'measured'-based and the analytically 'calculated' closure stresses, the analytically 'calculated' closure stress is divided by two since only the results for one patch were investigated experimentally.

Table 5.2: Comparison of measured and calculated maximum closure stress for a SMA-composite containing 11.8% V_f of SMA wires, h_s of 5 mm and h_p of 0.3 mm.

Pre-Strain(%)	$\sigma_c(max)$ (MPa)	
	measured	calculated($\div 2$)
0	0.73	0.18
1	3.14	1.09
2	2.85	2.18
3	3.26	3.27
4	3.14	4.36
5	3.12	5.45

N.B. "measured" means that the closure stress was calculated using the value for σ_r from experiments and equation 5.16, "calculated" is based on theoretically calculated value for σ_c using equation 5.13.

From this table it can be seen that the theoretically based closure stress is smaller than the experimentally based closure stresses for 0-2% pre-strain, and they show a reasonably good correlation between theory and experiment for a pre-strain of 3%. As the pre-strain increases, the theoretical σ_c(max) becomes larger than the experimentally based calculations. These differences occur since the recovery stresses obtained

from experimental data in Chapter 3 show very little variance with pre-strain, mainly due to the types of transformations occurring in the wires and the fact that the wires will continue to transform above 140°C (Section 3.7.1), whereas the analytical model assumes that there is an obvious linear change with respect to changing the pre-strain. Another reason for this discrepancy is that the patch is not being constrained at both ends in the analytical calculations, as in the experiment. Thus, the results obtained experimentally are the upper limit of the closure stresses which can be produced by a SMA-patch. The analytical results for low % pre-strain show a realistic result for the transfer of stresses.

It is also possible to calculate the expected recovery stresses of the SMA patch using the effective Young's modulus and effective pre-strain (given in equations 5.3 and 5.7). Table 5.3 shows a comparison between the analytically calculated and experimentally measured values (from Chapter 3) for different pre-strains and a V_f of 11.8% . The results differ because the analytical work is an estimate of what would happen if one of these SMA-patches were bonded along its entire length, to another structure. The experimental results are based on the recovery stresses of a SMA-patch, constrained at both ends and heated (see Chapter 3).

5.3.2 Variation of Patch Thickness

It is possible to optimise the patch thickness in order to obtain the largest closure stress possible. Figure 5.6 shows the closure stress in a 10 mm thick plate of aluminium for different SMA pre-strain values. From this figure it can be seen that the optimum patch thickness is around 0.3 mm. In real terms that corresponds to 2 layers of Kevlar fibre matrix pre-preg as used in Chapter 3. The reason that the data increases to a maximum and then decreases at around 0.3 mm is because as the patch thickness increases, the V_f of wires decreases to a point where the wires aren't as effective. It can also be seen that the greatest closure stress obtainable is for 5% pre-strain, which is to be expected.

With a patch thickness of 0.3 mm, it is also possible, practically, to embed several

Table 5.3: Table of experimental and calculated recovery stresses for a SMA composite patch with 11.8% V_f wires embedded.

Pre-Strain(%)	σ_r (MPa)	
	experimental	calculated
0	24.2	11.97
1	104.5	73.9
2	95.3	147.97
3	108.5	221.9
4	104.7	295.9
5	104.0	369.9

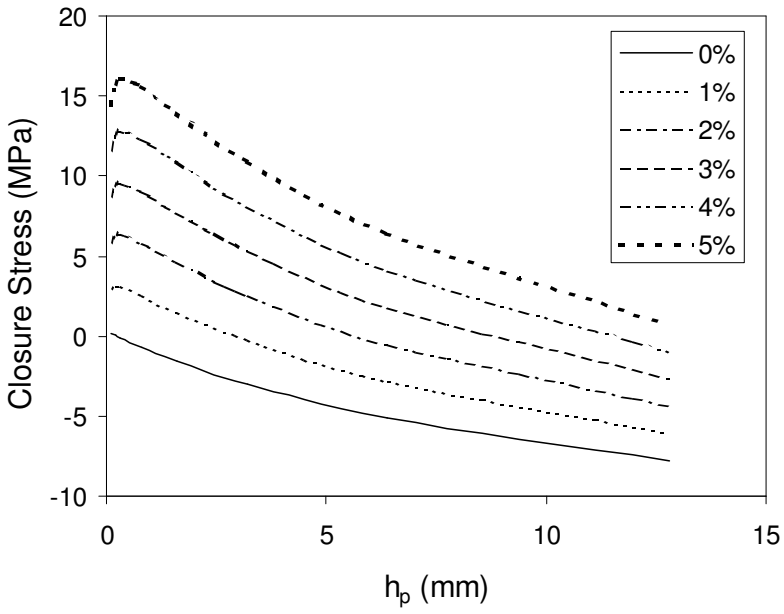

Figure 5.6: Closure stress versus patch thickness for varying pre-strain of SMA wires embedded in a composite patch and applied to a 10 mm thick Al plate.

Table 5.4: Material properties and closure stress for structures with h_s=10 mm, h_p=0.3 mm, 5% pre-strain and a V_f of SMA wires of 11.8%

Material	E_s(GPa)	σ_c (MPa)
Aluminium	70	10.84
Steel (mild)	210	10.97
Brass	100	10.90
Titanium	112	10.91
Epoxy	4	8.48
Alumina (ceramic)	382	10.99
Melamine formaldehyde	9	9.73
Concrete	18.5	10.36

more layers of SMA wires. Thus increasing V_f of the SMAs in the patch will also increase the closure stresses obtainable. Practically speaking, it should be possible to embed at least two layers of SMA wires, with a spacing of 2 wires/mm, thus possibly achieving a closure stress of 42.8 MPa for a 0.3 mm thick patch, corresponding to a V_f of 23.6%, with wires pre-strained to 5%.

5.3.3 Variation of Structure Material

Other material types, including steel, concrete, were also investigated to obtain an idea of the effectiveness of the SMA-patch on different materials.

The closure stress for a SMA-patch applied to different materials was determined. A patch with 11.8% V_f, with a pre-strain of 3% and thickness 0.3 mm was used and the structure was assumed to be 10 mm thick. The material properties and closure stress results are shown in Table 5.4.

5.4 Finite Element Modelling

A FEM, using the commercial software packages MSC Patran and ABAQUS, was developed in order to determine the feasibility of using a SMA patch to close cracks in structures. The FE results were also compared with the analytical model outlined in Section 5.2. A two-dimensional finite element model was developed, consisting of a structure with a SMA-patch applied with an adhesive layer. The SMA patch was modelled in two different ways.

The first model, which shall be known herein as the analytically based FEA, consisted of a SMA layer with an effective Young's modulus, given by equation 5.3, and an effective coefficient of thermal expansion derived from equation 5.7 and given by equation 5.17.

$$\alpha_{eff} = -\frac{1}{\Delta T}\left[\frac{\rho_{sma}(\epsilon_{ps}+\epsilon_{sa})+(1-\rho_{sma})\eta_m\epsilon_{ma}}{\rho_{sma}+(1-\rho_{sma})\eta_m}\right] \tag{5.17}$$

The areas, A_T, A_M and A_{SMA} involved in the calculations for α_{eff} and E_{eff} were determined by considering a patch of width 10 mm and wires of diameter 0.15 mm.

The second model, known herein as the experimentally based FEA, consisted of determining an equivalent strain based on the experimental recovery stresses, σ_R, and experimental coefficient of thermal expansion of the SMA-composite obtained in Chapter 3 (Table 3.11). From this an equivalent Young's modulus for the SMA patch was determined. Thus, when the attached patch is modelled using known recovery stresses an accurate estimate of the closure stresses is expected.

Table 5.5 shows the material properties used in the FEM. To take into consideration the effect of the contraction of the wires, the coefficients of thermal expansion of the aluminium and adhesive layers were taken to be zero. This is feasible since, as a first estimate, the recovery stresses obtained from the contracting SMA-patch and stresses transferred into the underlying structure are the properties of interest. Any thermal

Table 5.5: Material properties for FEM

Material	E_m (GPa)	α_m (/°C)	ν
SMA	62.7	11×10^{-6}	0.33
Kevlar matrix	33.5	-3.6×10^{-6}	0.33
Aluminium structure	70	0	0.33
Adhesive	2.8	0	0.36

effects regarding the aluminium and adhesive layer would have to be considered in detail at a later stage, once the feasibility of the SMA-patch is established. There are also issues as to how the wires are to be activated, ie. what methods of heating would be used in order to ensure that the aluminium and adhesive layers may not be affected by thermal effects. Thus, in order to simplify this process, the thermal effects of the adhesive and aluminium layers were considered to be negligible.

A model of the SMA patch applied to an aluminium plate (total thickness = 10 mm) was investigated, as illustrated in Figure 5.7(a). Since the use of the patch requires that it be applied on the top and bottom surfaces of an aluminium structure, to prevent unnecessary bending, a one quarter FE model of the system was used, as shown in Figure 5.7(b).

The aluminium plate and SMA patch were constrained along the planes of symmetry and the transfer forces were obtained along the patch/aluminium interface and along the x=0 axis of the aluminium. A 2D shell model of quadrilateral elements was used. Two load cases were considered, the first where the aluminium plate had no load, in order to compare the axial stresses with the closure stresses obtained using the analytical model, and the second case where the aluminium plate was loaded such that the maximum stress around the centre of the plate was 256 MPa, which is typical of the

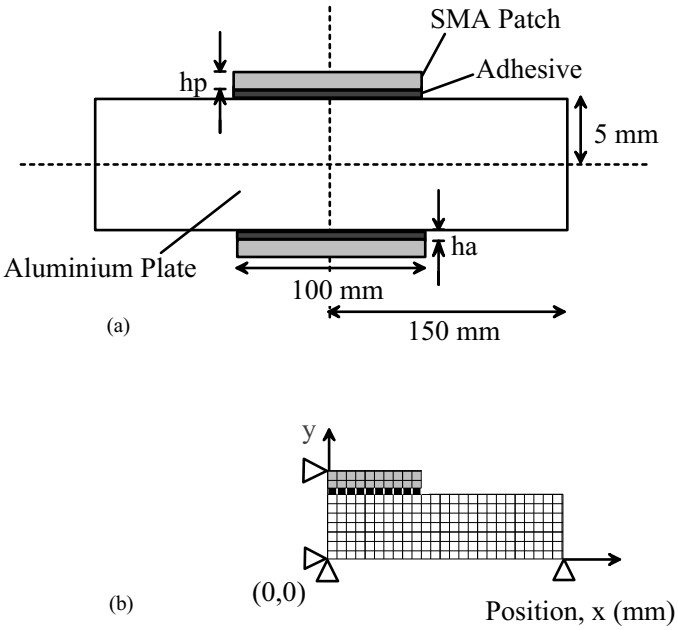

Figure 5.7: Schematic of the SMA patch attached to an aluminium plate and the one-quarter model used in the FE analysis.

maximum allowable stress for aluminium aircraft structures (Preston *et al.*, 1996). The SMA was then activated ($\Delta T = 60°C$) and the stress distribution in the aluminium was compared to that without the SMA activated. The axial stresses, σ_x, along the axis of symmetry (y=0) of the aluminium structure were investigated, along with the axial, σ_x, and shear, σ_{xy}, stresses between the patch and the structure. Parameters that were investigated include the effect of changing the thickness of the adhesive, h_a, variations in % V_f of SMA wires of 2.95, 5.9, 11.8 and 100% (which correspond to embedding 0.5, 1 and 2 wires/mm and a full SMA layer, ie. no matrix in the patch, respectively) and variation of stress with different pre-strain of SMA.

5.5 Results and Discussion of FE Modelling

5.5.1 Effect of Adhesive Layer on Stress

Figure 5.8 shows the effect of adhesive layer thickness on the axial stress at the centre of the aluminium structure (y=0) and the shear stress at the edge of the patch. A maximum pre-strain of 5% was used with a V_f of 11.8%. From this it is clear that an

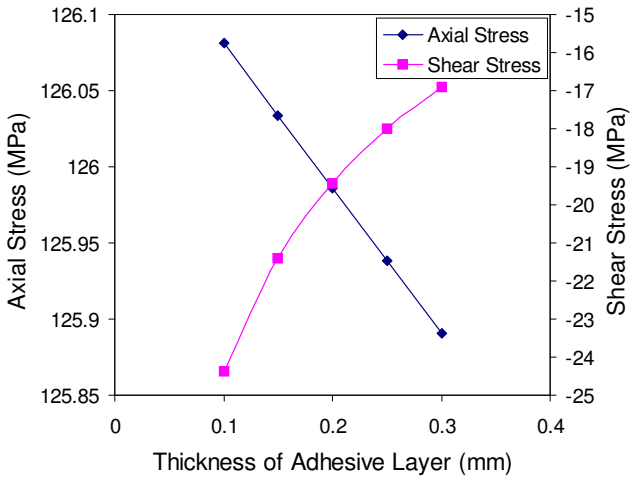

Figure 5.8: FEM results showing axial stress at the centre of the aluminium structure and shear stress at the edge of the SMA patch versus thickness of adhesive layer for a SMA composite with V_f of SMA wires of 11.8% and a pre-strain of 5%.

adhesive layer thickness of 0.3 mm produces the smallest shear stress and that there is not a large effect on the transferred axial stresses at the centre of the plate with differing patch thickness. Thus, for the rest of the FEM, an adhesive thickness of 0.3 mm was used in order to minimise shear stresses obtained at the patch edge.

5.5.2 Variation of Volume Fraction and Pre-Strain of SMA Wires

Different volume fractions of SMA wires embedded into the Kevlar patch were investigated for 2.95, 5.9 and 11.8%. The results for the load case with 0 load applied to the aluminium are shown in Figure 5.9. Figure 5.9(a) shows the axial stresses at (0,0) (the centre of the aluminium plate) produced with varying % pre-strain for both the numerical case (solid line) and the analytical case (dashed line). It shows that as the V_f increases, the effect of recovery stress of the wires becomes more pronounced and there is a greater difference observed between the analytical and the numerical results (Figure 5.9(a)). This difference could be due to the assumption of an effective coefficient of thermal expansion for the SMA due to the complex nature of the SMA-composite

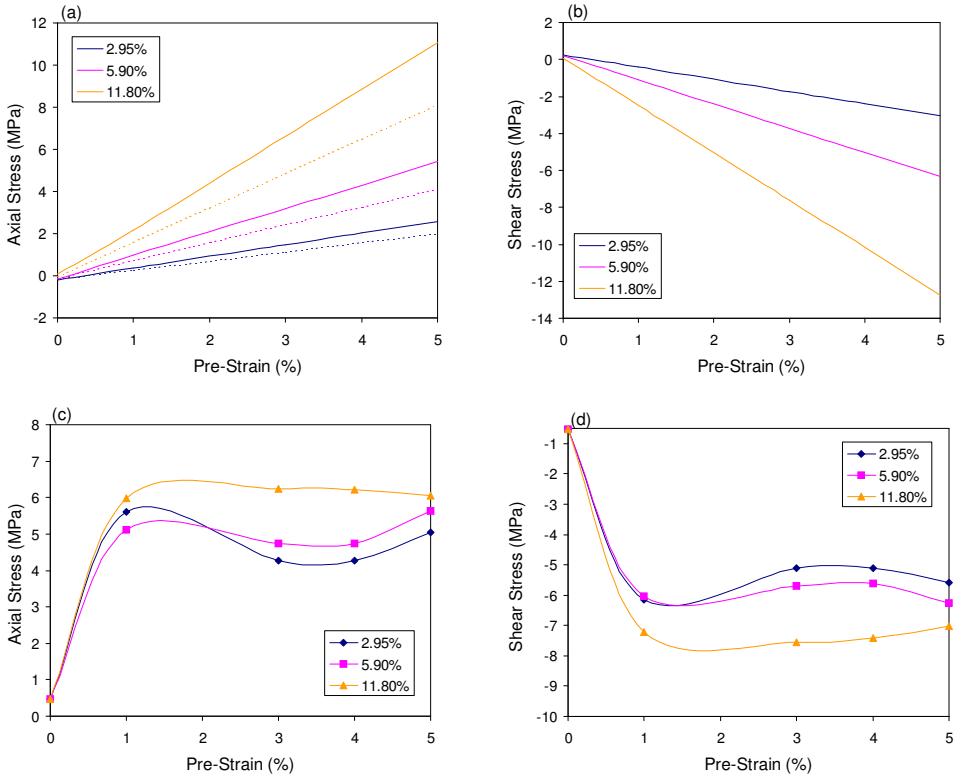

Figure 5.9: Variation of (a) axial stress at (0,0), (b) shear stress at edge of patch with varying % pre-strain for differing V_f of SMA wires for analytical based FEA and (c) axial stress at (0,0) and (d) shear stress at edge of patch with varying % pre-strain for differing V_f of SMA wires for experimentally based FEA.

thermomechanical behaviour. Figure 5.9(b) shows that as the % pre-strain increases, the shear stress at the edge of the patch also increases, which is to be expected. The equivalent charts for the experimentally based FEA for recovery stress are shown in Figures 5.9(c) and (d). It is shown that the behaviour is quite different to that of the analytical based FEA. The stresses tend to level out with differing pre-strain. This was explained in Sections 3.5.4 and 3.7.1, where recovery stresses continue to increase above 140°C. However, due to the interface between the wire and the matrix pulling away, there are constraints on how high a temperature SMA-composites can be heated to.

Figure 5.10 shows the results of stresses for varying % pre-strain for an applied

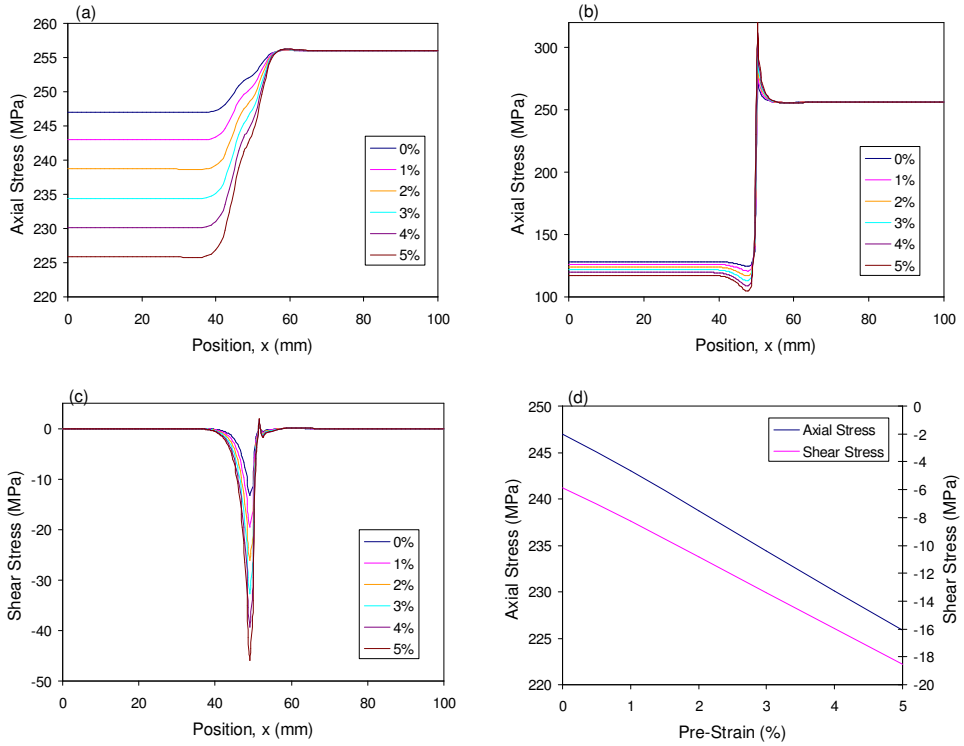

Figure 5.10: Results of analytically based FEA for varying % pre-strain of SMA wires embedded with a V_f of 11.8% and a patch thickness of 0.3 mm. (a) Axial stress along the y=0 axis, (b) axial stress along the patch/plate interface, (c) shear stress along the patch/plate interface and (d) summary of the axial stress along the y=0 axis and shear stresses along the patch/al interface. An external stress of 256 MPa was applied to the aluminium plate.

stress of 256 MPa on the aluminium structure. From Figure 5.10(a) it can be seen that as the % pre-strain is increased the axial stresses at the centre of the aluminium specimen (y=0) decrease.

Figure 5.10(b) shows that the axial stresses along the patch/plate interface, decrease from 128 MPa to 117 MPa for 5% pre-strain, but the shear stresses are very large at the edge of the patch (Figure 5.10(c)). The summary of stresses shown in Figure 5.10(d) indicates a linear relationship between the stresses and pre-strains, based on the analytical model.

Figure 5.11 shows the results of FEM based on the experimental results from Chapter 3. Shown are the axial stresses at the centre of aluminium structure,(0,0), as well

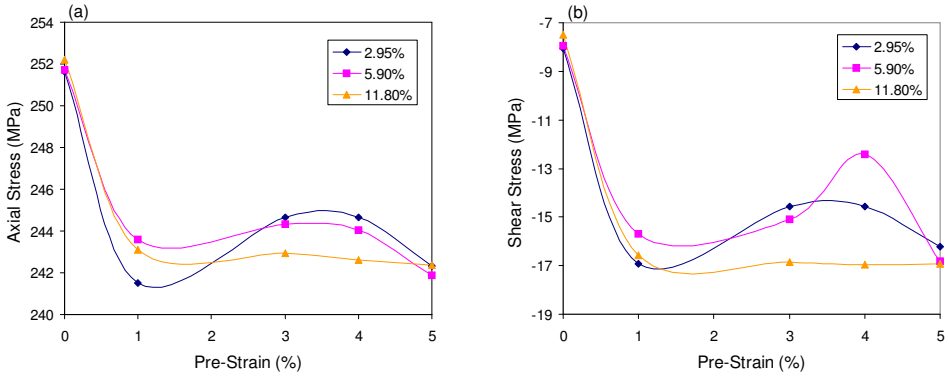

Figure 5.11: Results of experimentally based FEA for varying % pre-strain of SMA wires embedded with varying V_f and a patch thickness of 0.3 mm. (a) Axial stress at centre of the aluminium structure, (0,0), (b) shear stress at edge of patch. An external stress of 256 MPa was applied to the aluminium plate.

as the shear stress at the edge of the patch (at the patch/aluminium interface). From these it can be seen that the results tend to level off once again similar to the patch with no force applied to the structure. The shear stresses also tend to level off at the edge of the patch with a maximum of 17 MPa for 11.8% V_f.

Figure 5.12 shows the axial and shear stresses obtained for different V_f of SMA wires for the analytical based FEM model. Figure 5.12(a) shows that as the number of wires embedded is increased, the axial stress along the centre of the aluminium plate (y=0) decreases from 242 MPa to 225 MPa for a V_f of 11.8%. If, instead of using a SMA-composite, a SMA plate of 0.3 mm thickness is applied to a structure, it can be seen that there is a dramatic decrease (of 74%) in the axial stresses observed. However, as shown in Figure 5.12(b) and (c), the axial and shear stresses along the interface of the patch and plate at the edge of the "patch", increase to 597 MPa and 138 MPa, respectively. Figure 5.12(d) shows a summary of these stresses. For SMA-composite patches the axial stresses reach a maximum of 242 MPa and shear stresses reach a maximum of 34 MPa (for 11.8% V_f).

As well as the high shear stresses in the adhesive and high tensile stresses in the structure at the edge of the patch, high peel stresses would be induced in the adhesive

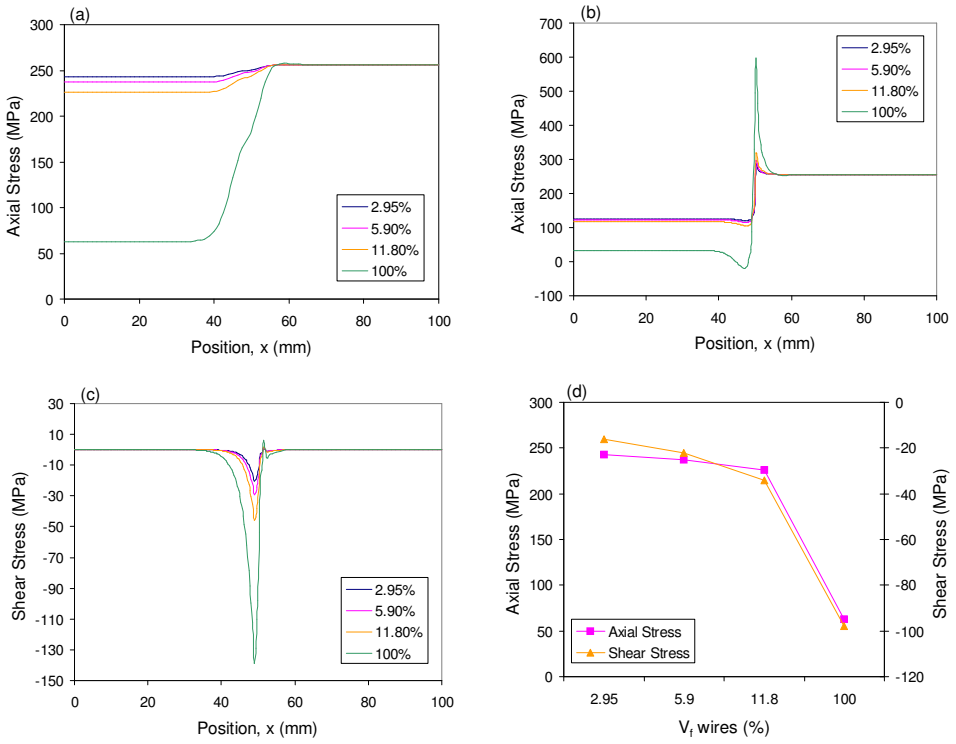

Figure 5.12: Results for varying V_f of SMA wires for analytically based FEA. (a) Axial stress along the y=0 axis, (b) axial stress along the patch/plate interface, (c) shear stress along the patch/plate interface and (d) summary of the axial stress along the y=0 axis and shear stresses along the patch/al interface. An external stress of 256 MPa was applied to the aluminium plate and a patch of thickness 0.4 mm and pre-strain of 3% was used.

layer at the edge of the patch when the SMA is activated. However, these can be minimised to some extent by correct design of the patch, such as tapering the edges. This stress concentration will also be weakened by the adhesive layer when the patch is bonded to the structure. It should also be noted that there are limitations to using an elastic model for determining the shear stresses on the adhesive layer. The elastic finite element analysis assumes that there is no yielding in the adhesive layer, that the behaviour of all the components is linear and that the overall deformations are small enough not to affect the stiffness matrix. In reality, when the shear stresses reach the yield point, the adhesive layer will exhibit visco-plastic behaviour which is dependant on the loading rate, and the strain levels in the adhesive are dependent on the load history. This visco-plastic behaviour needs to be taken into account for further analyses. However, in reality, such high shear stresses as to produce yielding, by activation of the SMA-composite patch, wouldn't be observed and, as such, the elastic model is a good first approximation.

5.6 Conclusion

From the results shown in this chapter it was observed that the closure stress in a cracked structure, due to SMA recovery stresses can be given by equation 5.13. From this the maximum closure stresses using SMA patches were obtained and compared with the results of recovery stresses determined from Chapter 3. By varying the V_f of SMA wires, the patch and structure thicknesses and the structure material properties different optimum closure stresses can be determined. There was some discrepancy between the experimental and analytical results for the recovery stresses.

Finite element analysis of the SMA patch applied to an aluminium structure was also carried out for analytically based and experimentally based cases. It was shown that for the analytically based FEM, as pre-strain and $\%V_f$ increased, the axial stresses at the centre of the aluminium structure and the shear stresses at the edge of the patch both increase. The experimentally based FEM showed that the stresses tended to level

off with increasing $\%V_f$ and pre-strain. However, for both cases, the axial stresses at the centre of the aluminium structure did decreases when the SMA-patch was applied and activated, thus showing the potential for using a SMA-patch to reduce stresses in a structure.

However, in order to determine an optimum patch a combination of V_f and % pre-strain needs to be considered, while taking into account the level of the shear and axial stresses that are obtained between the patch and plate surface. Correct design of the patch will also aid in reducing the stresses observed along this interface. As such a combination of both analytical and numerical modelling is required in order to properly understand the nature of the recovery stresses in the SMA-patch and the effects these stresses will have on a structure, in particular the behaviour of shear stresses at the edges of the patches.

As mentioned earlier, there was a discrepancy between the experimentally-based and analytically-based results. This gives a good indication that a simple linear elastic model isn't always appropriate since SMAs and their recovery stress behaviour don't behave in a linear manner. There are more complex issues involved in the recovery of the SMAs and these need to be incorporated into any model which is developed. However, in order to obtain a simplistic view of what would happen for different applications, a linear elastic model can be used as a good first estimate. Here it was shown that there is potential for using SMA-patches for reducing stresses in structures.

Future work would include an experimental investigation of the application of such a SMA-patch experimentally, in order to determine improved fatigue life of structures with existing cracks. Important aspects that need to be considered in an experimental investigation include determining the correct taper of the patch in order for there to be a minimum shear at the edge of the patch. Also the determination of the best way to activate the SMAs, either by heat or electric current and the effect this heating has on the adhesive layer and underlying structure would need to be investigated.

It would also be advantageous to try and develop an analytical model which incorporates the non-linear thermomechanical and transformational behaviour of the SMAs, in order to better model the use of SMAs and SMA-composites for different applications.